Spring 2017

# The Thermoelectric and Transport Properties of ZnSnN2

John Cenker
*John Carroll University*, jcenker17@jcu.edu

# The Thermoelectric and Transport Properties of $ZnSnN_2$

John Cenker

May 16, 2017

**Abstract:** Zinc Tin Nitride ($ZnSnN_2$) is the II-IV-$V_2$ semiconductor analog to the III-V Indium Nitride (InN), and the two are predicted to have similar properties that make them attractive for thermoelectric and photovoltaic applications. Replacing the costly and rare indium with more Earth-abundant and inexpensive zinc and tin makes $ZnSnN_2$ a potentially valuable alternative to InN. In this work, the temperature dependence of the Seebeck coefficient, Hall coefficient, and electrical resistivity were measured in a range of 7-300K. The Hall and resistivity measurements enabled the determination of Hall mobility and carrier concentration. Using the solutions to the Boltzmann transport equations in the relaxation time approximation and assuming a parabolic band, bounds on density of states effective mass are determined corresponding to different possible electron scattering mechanisms. The results show that samples with carrier concentrations around $6\text{-}9\times10^{19}$ $cm^{-3}$ exhibit properties consistent with the model, but not samples with a higher concentration of $1.02\times10^{21}$ $cm^{-3}$.

**Introduction:**

Behind the rise of modern technology has been an incredible jump in the ability to manufacture new materials such as semiconductors. However, many of the most commonly used semiconductors rely on rare elements which are hard to recycle. As a result, a pressing need has risen for semiconductors that utilize more common elements. One such semiconductor is $ZnSnN_2$ which is composed of elements that are orders of magnitude more abundant than its analog InN, which is a desired semiconductor due to its band gap energies which provide for important optoelectronic applications.[1] Furthermore, the procedures for recycling zinc and tin are already commonplace, whereas the mechanisms for recycling materials like indium and gallium are not yet well developed.[2] As a result, replacing InN with $ZnSnN_2$ could have green energy applications. However, since this material has so far only been grown by molecular beam epitaxy and has only existed since around 2011,[1] many of the properties of $ZnSnN_2$ remain unexplored. In addition, the literature suggests that $ZnSnN_2$ has two phases, an ordered orthorhombic and a wurtzitic structure which may have different properties[3].

One of the most fundamental electronic properties of a material is effective mass. It is essentially a correction to the free electron's mass due to the electron moving through a lattice instead of a vacuum. In order to determine effective mass from carrier transport measurements, four coefficients are needed. These coefficients are carrier concentration, Seebeck coefficient, electrical conductivity, and Nernst coefficient. The four coefficients each correspond to properties of the semiconductor[4]. With four coefficients, the effective electron mass can be determined. However, the Nernst coefficient has been shown to be too small to measure for these samples in previous results. As a result, only bounds on effective mass can be found in this experiment using the other three coefficients. In this work, the Hall coefficient, Seebeck

coefficient, and electrical conductivity are used to find the bounds on the effective mass for the different possible electron scattering modes. Then, these results can be compared to what a general model of the solutions to the Boltzmann transport equations would predict.

**Theory:**

The first property needed for finding the bounds on the effective mass is electrical conductivity, $\sigma$. Conductivity is defined as the ratio of the current density to the electric field used to induce it. As a result, materials with high conductivity will conduct electricity better as they will have a large current even with a small electric field. The microscopic formula for electrical conductivity is given by:

$$\sigma = ne\mu \tag{1}$$

where $n$ is the carrier concentration, $e$ is the charge of the electron, and $\mu$ is the electron mobility in the sample. Conductivity is a bulk scale property, which arises because of the microscopic properties of carrier concentration and mobility. Since it depends on both carrier concentration and mobility, if conductivity and one of $n$ or $\mu$ is also measured, the other can then be determined.

The second coefficient, the carrier concentration, gives the number of mobile charge carriers per unit volume and is found using the Hall Effect. The Hall Effect occurs when a current is moving in the presence of a perpendicular magnetic field. Moving charges subject to a perpendicular field will feel a magnetic force leading to the buildup of charge carriers on one side, which also causes the other side to become oppositely charged. This buildup of charge carriers produces an electric field and thus a voltage. Using the transverse voltage that results due to this effect, the Hall resistance can be found using Ohm's Law. Using the Hall resistance, the

thickness of the sample, and the applied magnetic field, the carrier concentration, $n$, can be found using the following relation:

$$R_H = \frac{B}{nqd} \tag{2}$$

Here $d$ refers to the thickness of the sample, $R_H$ refers to the Hall resistance, and $B$ refers to the magnitude of the applied $B$ field. Essentially, $B$ is varied and $R_H$ is measured. The slope of the $R_H$ vs $B$ curve is then used to find carrier concentration and mobility.

Mobility describes how easily the electron (or hole depending on the semiconductor) moves through the lattice. Using the measured carrier concentration and conductivity from Hall experiments, the mobility is determined from Eq. (1). As mobility gives insight into how charge carriers are scattering through the lattice, the temperature dependence of the mobility hints at which mode of scattering may be occurring.[5] As temperature lowers, scattering due to phonons is expected to decrease as the lattice vibrations become less. This dependence is proportional to $T^{-3/2}$. If there is no temperature dependence, then neutral impurity scattering would be indicated as the effects of neutral impurities are not dependent on temperature. A mobility that increases proportional to $T^{3/2}$ would correspond to ionized impurities.

The final coefficient needed for determining the bounds on effective mass is the Seebeck coefficient, which relates the potential difference across the sample to the temperature gradient producing it. When a temperature gradient is present, the fast moving electrons at the hot end diffuse to the cold end, forming a voltage difference across the sample. This coefficient is given by:

$$S = \frac{\Delta V}{\Delta T} \tag{3}$$

where $\Delta V$ is the voltage generated by the temperature difference $\Delta T$. As it relates the voltage produced to a temperature gradient, the Seebeck effect is an important thermoelectric property. Unlike the other coefficients, the Seebeck coefficient will change with temperature.

In this work, the conduction electrons in $ZnSnN_2$ are being modelled as a degenerate Fermi gas with one parabolic conduction band. Under this model, the mobility can be expressed as:

$$\mu = \frac{e\tau}{m^*} \tag{4}$$

where $e$ is the charge of the electron, $\tau$ is the charge scattering time, and $m^*$ is the effective mass. Another assumption of our model, known as the relaxation time approximation, is that $\tau$ has a dependence of $E^r$. That is,

$$\tau = \tau_0 E^r \tag{5}$$

where $\tau_0$ is a constant, $E$ is energy, and $r$ is the scattering coefficient. As electrons move through the lattice, there are different modes that may cause scattering. The scattering parameter $r$ corresponds to these different scattering methods: $r$ = 3/2 corresponds to ionized impurities, $r$ = 0 to neutral impurities, and $r$ = -0.5 to acoustic phonon scattering. Solving the Boltzmann transport equation under the above stated assumptions, the Seebeck coefficient can be theoretically expressed as:[4]

$$S = \pm \frac{\pi^2 k_B^2 T \left(r + \frac{3}{2}\right)}{3eE_F} \tag{6}$$

where $T$ is the temperature, and $E_F$ is the Fermi energy. In the degenerate Fermi gas model, the Fermi energy is defined by[4]:

$$E_F = \frac{h^2 \left(\frac{3n}{\pi}\right)^{\frac{2}{3}}}{8m^*} \tag{7}$$

where $n$ is the carrier concentration and $m^*$ is the effective mass. Manipulating these equations, the effective mass corresponding to the different scattering parameters can be extracted. Since $r$ is bounded by -1/2 and +3/2, the boundaries on the effective mass can be calculated.

**Experimental:**

**Table I.** The different growth parameters for the samples in this work.

| Sample | Growth Temp (°C) | Zn Flux [atoms/(s*cm$^2$)] | Sn Flux [atoms/(s*cm$^2$)] | $N_2$ Pressure (Torr) | RF Power (W) | Growth Time (Hours) |
|---|---|---|---|---|---|---|
| **A** | **450** | **$3.98\times10^{14}$** | **$1\times10^{13}$** | **$1\times10^{-5}$** | **150** | **1** |
| **B** | **450** | **$3.98\times10^{14}$** | **$1\times10^{13}$** | **$1.5\times10^{-5}$** | **150** | **3** |
| **C** | **420** | **$1.97\times10^{15}$** | **$3.22\times10^{13}$** | **$3.66\times10^{-5}$** | **300** | **5** |

In this study, we used three $ZnSnN_2$ samples grown using molecular beam epitaxy. Table I shows the different conditions under which each sample was grown. It is beyond the scope of this project to fully analyze how each of these parameters could possibly affect the electronic properties of the sample. However, that might be a future goal for the continuation of this research. The thickness of Samples A and B was given as 100 nm and the thickness of Sample C was given as 90nm. Since the uncertainty in the thickness of the sample has not yet been determined, the error in $n$ is also unknown. Further research into this question is needed in order to quantify our uncertainties.

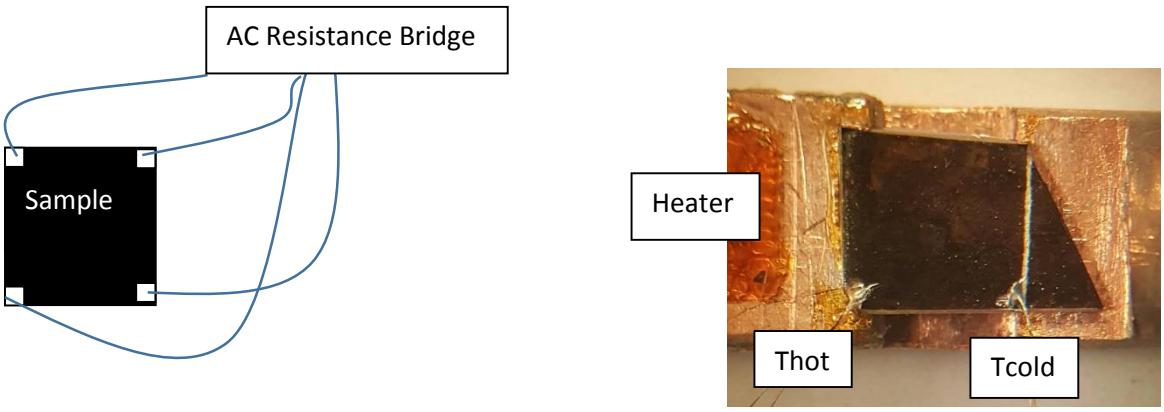


**(a)** Hall Measurements (Van der Pauw) **(b)** Seebeck Measurements

**Figure 1**. The schematic for **(a)** Van der Pauw style Hall and **(b)** Seebeck measurements.

The experimental part of this project is to measure the temperature dependent Hall effect, Seebeck effect, and electrical conductivity. These effects are measured at temperatures ranging from 7k to 300k. For Hall measurements, the magnetic field is generated with a Lakeshore electromagnet which produces a maximum field of around ± .7 T. The sample is cooled using a closed-cycle helium cryostat at a vacuum of $10^{-6}$ torr. The experimental setup for measuring the Hall Effect is shown in Figure 1. Indium contact points were soldered at the corners of the sample in a Van der Pauw configuration. Using copper wires soldered at 204°C to these contacts, different measurements and permutations of the resistance are taken with an excitation current of 10μA and at high vacuum using a Lakeshore AC Resistance Bridge. These different resistance readings were automated via a LabView program which performed the complicated Van der Pauw calculations and was then used to find the Hall resistance and conductivity. The carrier concentration can be found by using Eq. (2). During temperature dependent measurements, the LabView program measures sheet concentration, $n_s$. Since this sheet concentration is equal to the carrier concentration multiplied by the thickness of the sample, it can be used to find carrier concentration. Using the carrier concentration and conductivity, mobility can be determined.

The sample region of the apparatus showing the thermocouple and heater configuration for measuring the Seebeck coefficient is also shown in Fig. 1. A current is driven through the heater, which is essentially a 350Ω thin film resistor. This heater is mounted to the stage with GE 7031 varnish and connected to a Keithley Sourcemeter 2400. The result of this heating is a temperature difference from the hot end (closer to the heater) to the cold end ranging from 0.2-1.0 K. This temperature difference is determined by using the voltage readings from the copper-constantan thermocouples which are connected to Keithley 2182 nanovoltmeters. The potential difference across the sample is also measured with a Keithley 2182 nanovoltmeter by using the 25 micron-

diameter copper wire legs of the thermocouples. As with the Hall measurements, a Lakeshore temperature controller is used to measure the temperature dependence of the Seebeck effect at various temperatures and under high vacuum.

After the measurements are taken, the second part of this work is to compare the results of the new sample with previously obtained data to check for consistency. In order to do this, Eq. (6) is used to plot $S$ vs $n$ for different effective masses. These plots are generated using previously developed MathCAD code. Furthermore, the results of the temperature dependent Hall and Seebeck measurements are plugged into Eq. (6) and compared to the results of data taken in the summer.

**Data and Analysis**

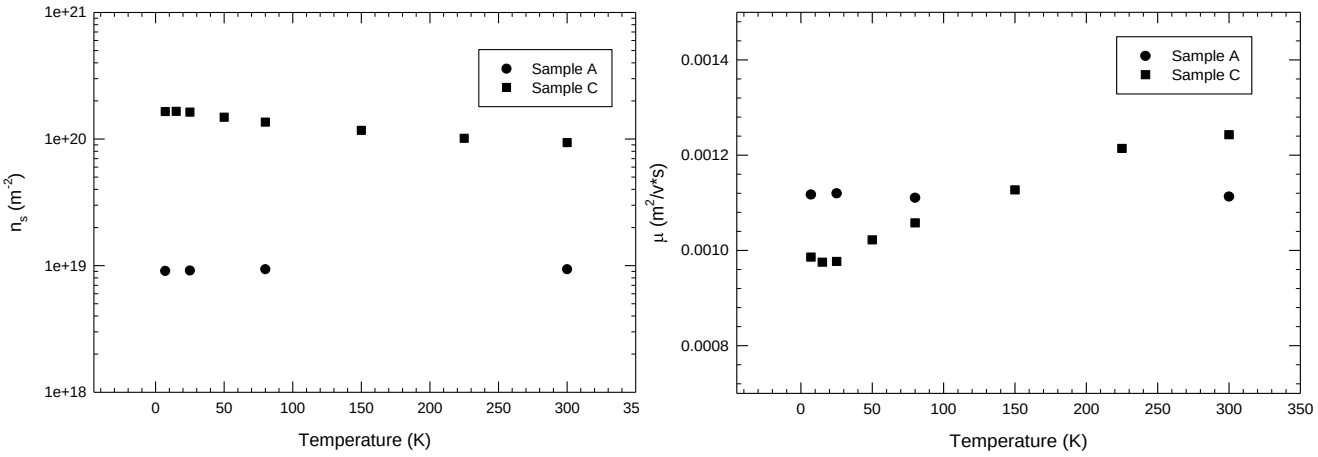


**Figure 2.** The results of sheet concentration and mobility as a function of temperature.

A consequence of the degenerate Fermi gas model being used is that carrier concentration should remain flat with temperature. Figure 2 shows the results of Hall measurements. The sheet concentration shown in Figure 2 is equal to the carrier concentration multiplied by the thickness, so it shows that $n$ for Sample A has no dependence on temperature. This provides evidence that the degenerate approximation is valid. Sample C shows more variation in temperature, which may

indicate that the model is not valid. Also, as shown in Table II, Sample C, which was measured this semester, has much higher carrier concentration than Sample A. One possible explanation for this variation in temperature is that under much higher doping level, a higher-lying conduction band is populated along with the lowest-lying conduction band. When it comes to mobility, Sample C displayed a similar mobility, but once again showed more variation with temperature. As mentioned before, the temperature dependence of the mobility provides insight into the scattering mode. As there is no temperature dependence for Sample A, it is likely that neutral impurity scattering dominates. Sample C, however, increases with increasing temperature which may indicate ionized impurity scattering in a single band, or participation of another band.

The electrical conductivity is also determined from the Hall measurements. Conductivity is the inverse of the resistivity, ρ. As a result, Sample C displayed a lower resistivity and thus a higher conductivity. The resistivities of all of the samples are shown in Table II.

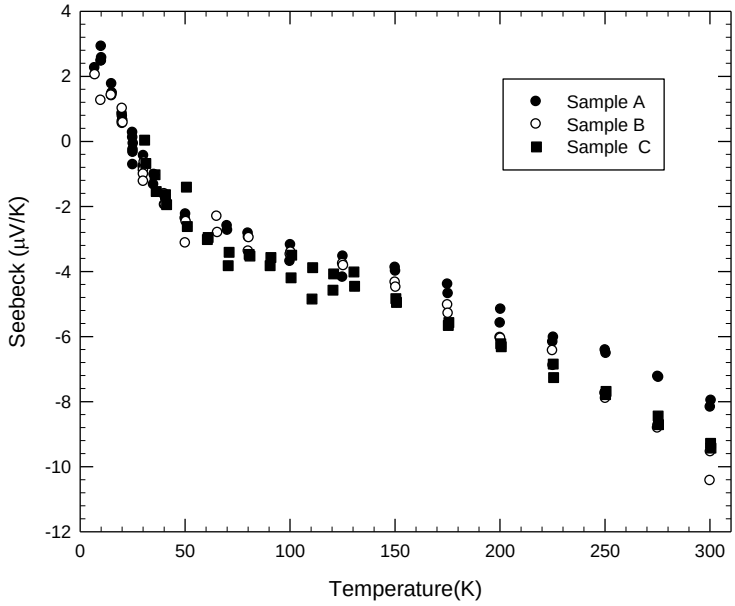


**Figure 3.** The results of Seebeck measurements through the whole temperature sweep.

Another important measurement was the Seebeck coefficient. Figure 3 shows the Seebeck coefficient that is used in Eqs. (6) and (7) to determine the bounds on effective mass. Despite having a much higher carrier concentration, Sample C demonstrated a Seebeck coefficient on par with the other samples. The low temperature Seebeck data for all samples actually displayed a switching of sign; the Seebeck was small, but positive, below around 20K. This could possibly indicate some sort of systematic error, and the system should be tested with a piece of superconductive material in order to determine the Seebeck effect due to the wires attached to the sample. However, this system for measuring Seebeck coefficient has been tested before with known materials and has produced reliable results. The switching in sign is something that could be studied further if this work were to be continued.

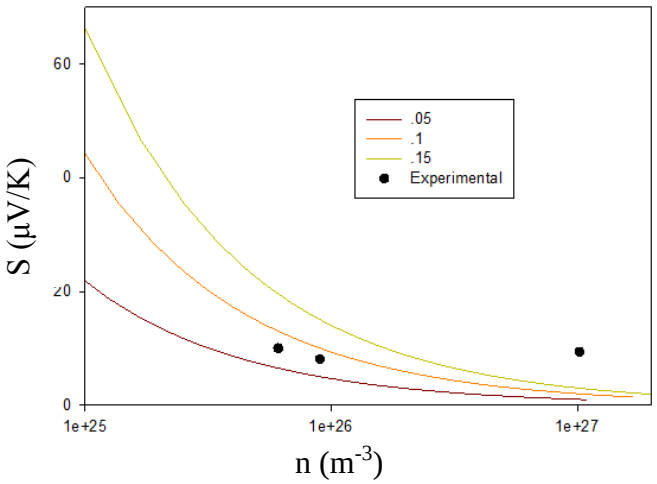


**Figure 4.** Seebeck coefficient vs carrier concentration for different effective masses, r = -1/2.

**Table II.** The measured properties of all Samples and the effective masses corresponding to different scattering parameters.

| | **n ($cm^{-3}$)** | **ρ (Ω*cm)** | **μ ($cm^2/V*s$)** | **Seebeck (μV/K)** | **$m^*$ for r=-1/2** | **$m^*$for r=3/2** | **$m^*$for r=0** |
|---|---|---|---|---|---|---|---|
| **A** | $9.01\times10^{19}$ | $5.98\times10^{-3}$ | 11.6 | 8.08 | 0.081 | 0.03 | 0.05 |
| **B** | $6.1E\times10^{19}$ | $6.65\times10^{-3}$ | 15.4 | 10 | 0.085 | 0.03 | 0.06 |
| **C** | $1.02\times10^{21}$ | $4.83\times10^{-3}$ | 12.7 | 9.36 | 0.45 | 0.15 | 0.3 |

Using a degenerate Fermi gas model of the Seebeck coefficient and carrier concentration generated last semester, a plot of Seebeck coefficient vs carrier concentration can be used to compare the theoretical predictions to experimental results. As phonons are an intrinsic phenomena and are always present in the lattice, this mode of scattering was used to generate the plots of Figure 4. Figure 4 shows that the experimental results for Samples A and B fit within the lines generated by effective masses of .05 and .1. When the model is fitted for Samples A and B, it clearly does not fit for Sample C. The reason for this is not quite clear yet, however it likely has to do with it's extremely high carrier concentration. It could mean that the assumption of the model that there is a single parabolic band is incorrect. Table II shows all of the room temperature data that has been collected on all samples. It also demonstrates that the bounds on the effective mass of Sample C are extremely higher than those of Sample A or B in this model.

According to the literature, $ZnSnN_2$ has two different phases: a wurtzitic and an ordered orthorhombic structure[3]. All of the samples measured in this work are likely the wurtzitic phase. Figure 4 shows that, according to the model, the Seebeck coefficient should get much larger at lower carrier concentrations. As a result, study of samples exhibiting the orthorhombic structure, which is expected to have a different carrier concentration, would provide key insights into whether the model holds up and the veracity of the data. These different phases could possibly be identified using further x-ray diffraction analysis.

**Conclusion:**

Charge and heat transport measurements were performed on three samples of $ZnSnN_2$. All three samples exhibited similar Seebeck coefficients despite one having significantly higher carrier concentration. Under a degenerate Fermi gas model with a single parabolic band and a relaxation time approximation, the effective mass of samples with carrier concentrations around

6-9×10 $^{19}$ cm$^{-3}$ ranged from .03 to .085 times the mass of a free electron. The sample with the higher carrier concentration does not fit the model, possibly indicating a different band structure. More samples, especially those with low carrier concentrations, are needed to test the strength of the model and to gain more insight into the electronic properties of $ZnSnN_2$.

**References**:

1. N. Feldberg, J.D. Aldous, W.M. Linhart, L.J. Phillips, K. Durose, P.A. Stampe, R.J. Kennedy, D.O. Scanlon, G. Vardar, R.L. Field, T.Y. Jen, R.S. Goldman, T.D. Veal, and S.M. Durbin, Appl. Phys. Lett. **103**, 042109 (2013).

2. N. Feldberg, B. Keen, J.D. Aldous, D.O. Scanlon, P.A. Stampe, R.J. Kennedy, R.J. Reeves, T.D. Veal, and S.M. Durbin: ZnSnN2: a new earth-abundant element semiconductor for solar cells. *Proc. of the 38th IEEE Photovoltaic Specialists Conference*, Austin, TX, p. 2524 (2012).

3. A. N. Fioretti, A. Stokes, M. R. Young, B. Gorman, E. S. Toberer, A. C. Tamboli, A. Zakutayev, Adv. Electron. Mater. **3**, 1600544 (2017).

4. Nolas, G.S., Sharp, J., and Goldsmid, H.J., *Thermoelectrics: Basic Principles and New Materials Development*, Springer, Germany, 2001

5. Putley, E. H., *Hall Effect and Related Phenomena*, Butterworths, London, 1960.